*David Barland AFRL*

*Brian Williams Ultramet*

# Strength and Permeability Properties of Ceramic-Coated and Uncoated Porous Refractory Cellular Materials

## *Abstract*

Uncoated and ceramic-coated porous cellular foams of moderate (60%-95%) porosity were experimentally investigated to determine strength moduli and gas permeability. Uncoated porous samples consisted of reticulated vitreous carbon (RVC) rigidized by pyrolysis of flexible, open-pore organic precursor foams. The organic precursor's reference surface pore density was 100 pores-per-inch (ppi) before uniaxial compression. After compression, substrates contained 6% to 33% solid fraction, which corresponded to 200 ppi to 1100 ppi, respectively. To construct ceramic-overlaid samples, the 600 ppi and 1000 ppi substrates were coated with silicon carbide to 5% and 12% additional densities via chemical vapor infiltration (CVI). Anisotropic mechanical strength was measured in compression for all materials. In an attempt to correlate strength, density and flow resistance, anisotropic gas permeability was measured using a differential pressure measurement apparatus with pore-scale Reynolds numbers ranging from 3 to 200. Results showed compressive crush strengths bounded between theoretical strengths of solid RVC substrate and SiC coating materials. The data may be applied to allow more efficient design of ceramic-coated porous cellular materials with variable coating thickness.

## INTRODUCTION

Many modern concepts in thermal protection systems, transpiration-cooled rocket and scramjet combustor and nozzle liners, fluidized bed and filtration combustion, and lightweight high-temperature structures seek integration of open-pore refractory materials. Practical application of high-temperature porous media requires that the collected properties of porosity, temperature resistance, specific strength, and durability provide a working, cost-effective solution that solves the unique requirements of an application, or provides a unique solution to an existing problem. In thermal protection skins and combustor liners, for example, heat fluxes and oxidation vulnerability, conventionally mitigated by passive ablation or convective cooling through permeable sintered metal walls, can be further reduced to by integrating lightweight refractory porous materials with much higher use temperatures and

finely distributed pores. Ideally, open-pore cellular foams can be engineered for a given application by optimizing the defining variables of density, porosity, and pore distribution by altering the precursor's compression or subsequent ligament coating.

By changing the shape, density, structure and distribution of pores, a material property can be designed to specific requirements. For example, fluid dispersion and mixing is greatly intensified within foams by creating tortuosity, which is a consequence of the high pore densities attained by precursor compression.

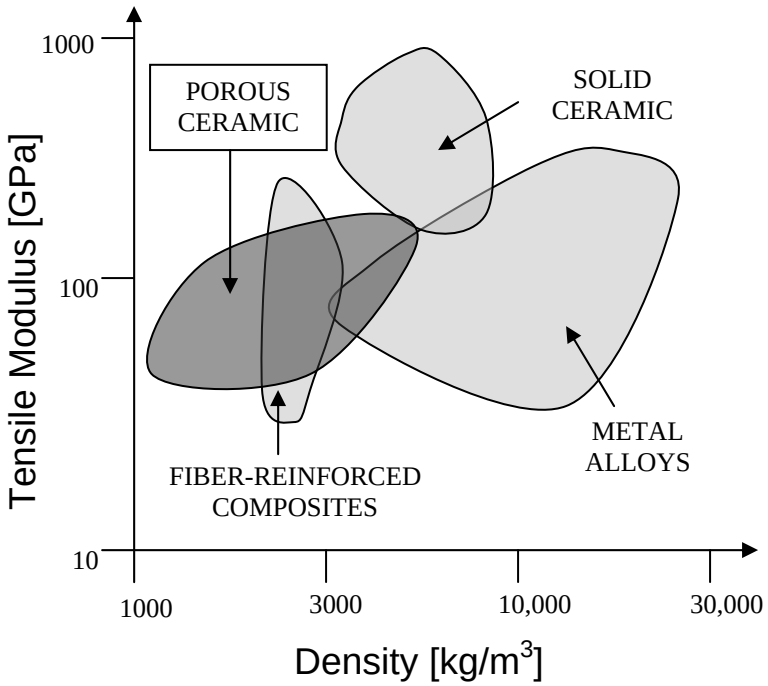


**Figure 1** From Ashby (1992), grouping high modulus materials by class. The range of porous ceramics is extended to cover common cellular materials.

The three major classes of modern engineered refractory porous materials, i.e., sintered, cellular, and fiber reinforced composite (FRC), cover broad ranges of porosity and mechanical strength. Following Ashby (1992), Figure 1 illustrates the expected range of mechanical strength and density of porous ceramics in comparison to other high modulus material classes. The selection or substitution of a refractory porous ceramic begins with choosing a

compromise between required strength, sustained use temperature, anticipated expansion coefficients, porosity, etc., and continues by optimizing the plethoric supply of interwoven dependencies and requirements such as permeability, thermal shock resistance, conductivity, ease of fabrication, fluid dispersion and mixing efficiency, inertness, ablation resistance and so on. A motivation of the current research is that, in comparison to sintered porous ceramics and organic composites, refractory cellular solids present a new generation of relatively strong, lightweight, high-temperature, moderately porous materials capable of solving problems in a wide variety of applications.

A refractory coating placed upon a cellular substrate produces a material that combines high porosity with a portion of the consolidated solid's strength. Coatings are accumulated uniformly throughout the ligament-based foam

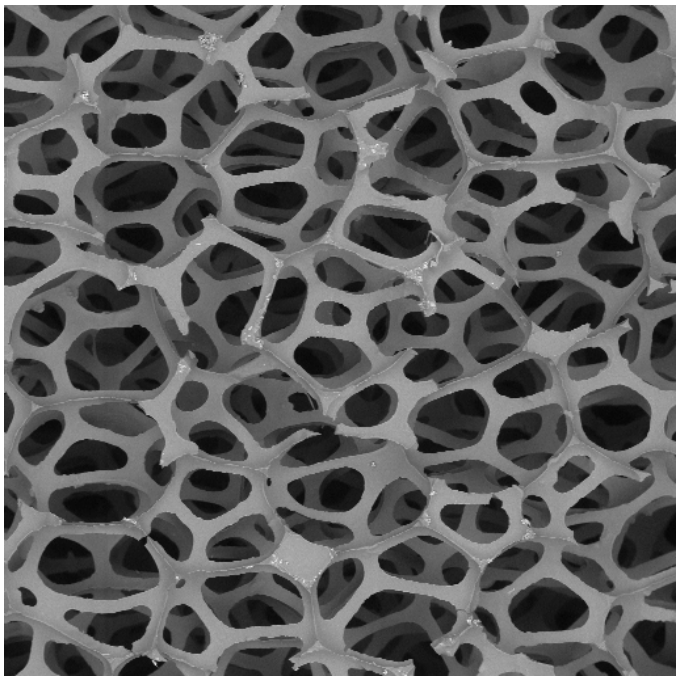

**Figure 2** SEM micrograph (49X) of uncoated, uncompressed RVC core of 100 ppi.

substra ) thereb npared to their uncoated core. Figure 2 displays the uncompressed, uncoated RVC foundation upon which all the subject material of this investigation rests. The skeletal structure is primarily notable for its indeterminacy and the predominance

**Figure 3** SiC-Coated 1000 ppi Cellular RVC material. Note the uniformity of the SiC deposition upon the underlying RVC ligaments in this 162X back-scattered SEM micrograph.

of irregular pentagonal pore faces. The micrograph of Figure 3 illustrates the even more indeterminate character that results from highly compressing and rigidizing an elastomeric precursor. The progression of pore collapse is illustrated by the micrographs of Figure 4.

If coated with a material of relatively higher specific properties, such as SiC, the foams rapidly take on the character and a meaningful portion of the moduli of a block of fully consolidated coating material. The primary strength-determining factor is well known to be the relative density, $\rho^* / \rho_S$, defined as the ratio of the mass density of the porous solid to that of the theoretical fully dense solid, and is equal to $1-\varepsilon$ for single-constituent materials, where $\varepsilon$ is the volumetric porosity. Therefore, the supposition exists that a substrate's composition, initial compression, and pore shape and distribution should have minor effect on isotropic mechanical properties. However, the laminated nature of

a solid-core coated cellular material requires careful application of empirical strength correlations. The (usually) relatively weak substrate may still be a large fraction of the total strength of thin coatings and may contribute the majority of the strength for highly compressed, lightly coated foams. Results will be

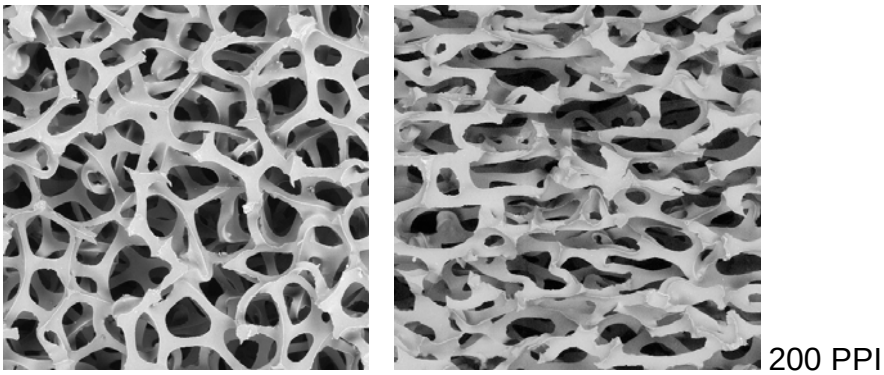
200 PPI

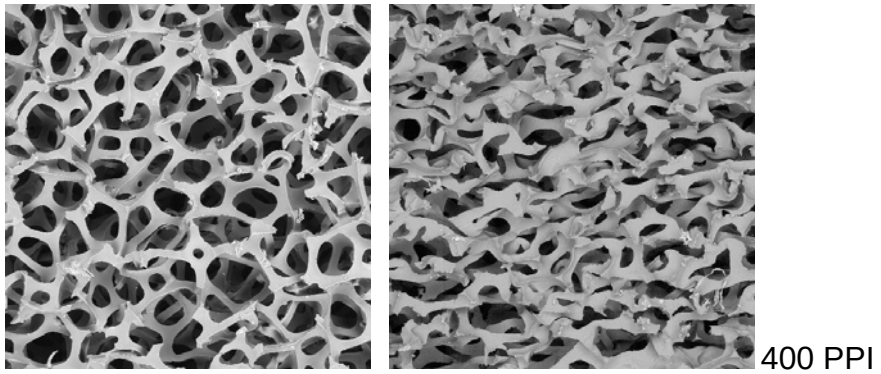
400 PPI

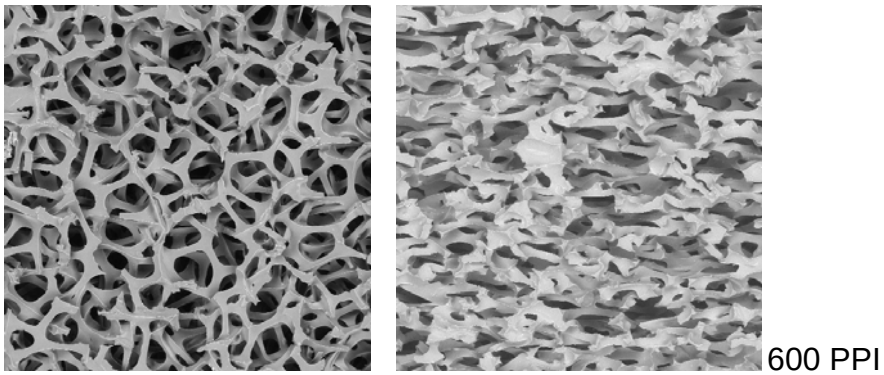
600 PPI

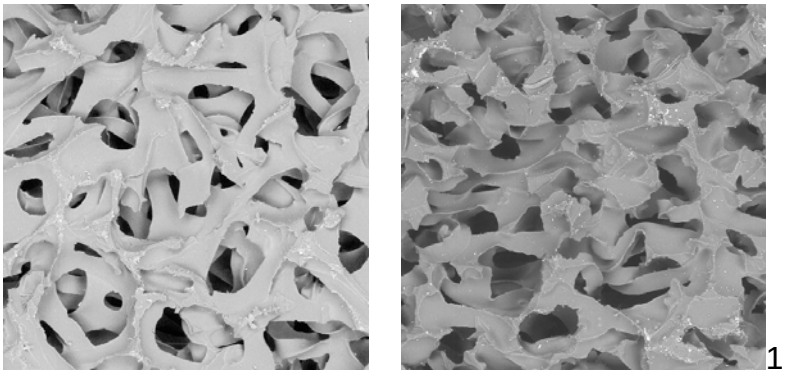
1100 PPI

**Figure 4** Progressive pore collapse of RVC foam created from uniaxial compression of 100 ppi RVC. The right column views are perpendicular to the plane of compression and illustrate progression of pore collapse. The left column views are of faces parallel to compression.

presented later to help quantify the (sometimes dominant) influence of core versus coating upon strength of compressed foams. Logically, even if the coating's substrate contributes little to strength, it still influences fluid flow tortuosity and surface area by defining the underlying pore-scale shapes and relationships.

Upon significant coating deposition, a cell's ligaments distend and are altered in both size and shape. Figure 5 illustrates the change in character of ligament boundaries with coating deposition, as the triangular-sectioned, sharp-cornered substrate distends and rounds, and surfaces may become nodular. The rounded corners of the as-deposited SiC most certainly has implication in flow resistance as quantified by permeability, as well as the ligament moment of inertia, which is germane to macroscopic strength relations.

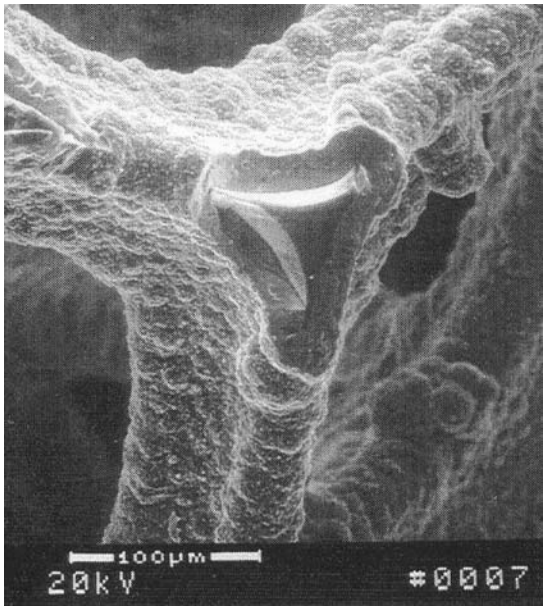


**Figure 5** Triangular cross-section of SiC-coated ligament. The underlying RVC core is clearly visible at the center.

The distension of the ligaments also serves to reduce pore volume, albeit as a minor fraction of pore volume until the substrate is highly compressed and thickly coated. For uncompressed foam of approximately 100 ppi (pores-per-inch), the initial pore diameter appears on the order of .010", but may reach as small as .001" to achieve, say, 1000 ppi. Stress response of cellular foams, while linear in both tension and compression over the small strain range where

ligaments bend but do not break, becomes highly nonlinear when rupture occurs. The normal difficulties in nonlinear analysis are exacerbated by the inherently anisotropic properties of compressed foams. In the terminology of Gibson and Ashby (1997), cells possess a measure of anisotropy called “shape-anisotropy” ratio *R*, which is defined simply as the ratio of maximum to minimum dimensions of a pore. Altering *R* by compression of the flexible precursor determines the anisotropy of properties (conversely, it should be possible, with care, to achieve nearly perfect isotropy through compression).

The uniaxial compression needed to produce a 600 ppi foam substrate from a 100 ppi precursor can create a very anisotropic material indeed, with principal moduli of the finished product predicted to vary up to a factor of 100. The variation in elastic modulus E due to shape-anisotropy is on the order of $R^2$; a goal of the present research is to characterize the effect of *R* upon fluid permeability as well. Evaluation of the effect of compression upon permeability is valuable in order to provide quantification of the permeability, $\kappa$, in anisotropic tensor form for design and analysis.

Macroscopic material properties, such as specific surface area, are employed in developing empirical models of viscous flow within porous materials. Kozeny (1927) provide the well-established permeability relation involving only a geometric correction factor $C_0$, the specific surface area $S$, and the porosity $\varepsilon$. Kozeny’s equation, $\kappa = C_0 \frac{\varepsilon^3}{S^2}$, and the relation of Brace (1977), $\kappa = Ad^2\left(1-\left(\rho^*/\rho_S\right)\right)^{3/2}$, where $A$ is an empirical constant and $d$ represents a pore diameter, are perhaps the most thoroughly investigated correlations of permeability to the properties of porous materials. The Kozeny and Brace equations are most appropriate for materials of high porosity, and specifically for flows of Reynold’s number below the transition to turbulence of $\mathrm{Re}$ ~100 for most foams. Meaningful empirical application of the Kozeny equation requires measurement of specific surface area $S$ to determine the geometric correction factor. While techniques exist to directly measure $S$, such as the BET method,

the representation of the permeability as a tensor means that the Kozeny correction factor will also be in tensor form. For design and analysis, direct measurement of permeability, as presented below, is recommended since few authors have developed validated multi-dimensional equations of fluid flow in porous media using an anisotropic permeability tensor (see Bear (1972)).

An explicit, homomorphic model of the geometry of even uncompressed foam is currently nearly intractable due to the indeterminate, three-dimensional nature of ligament topography. The inter-ligament relationships are complicated further by the compression of the organic precursor substrate prior to rigidization. An elastomeric foam, the organic precursor does not collapse in any orderly or predictable fashion upon compression. As shown in Figure 4, even for uncoated foam of only two-to-one uniaxial compression, the twisting and bending of ligaments results in a chaotic, yet plausibly directional, structure.

Approximate geometric representations consist of variations on Archimedean solids such as the dodecahedron or conception of space-filling shapes such as Kelvin's tetrakaidecahedron shown in Figure 6. The simplified but determinate geometric models give an idea of morphological complexity, but it is difficult to even conceive of the complexity of the solutions themselves if a microscopic geometry was applied to analysis.

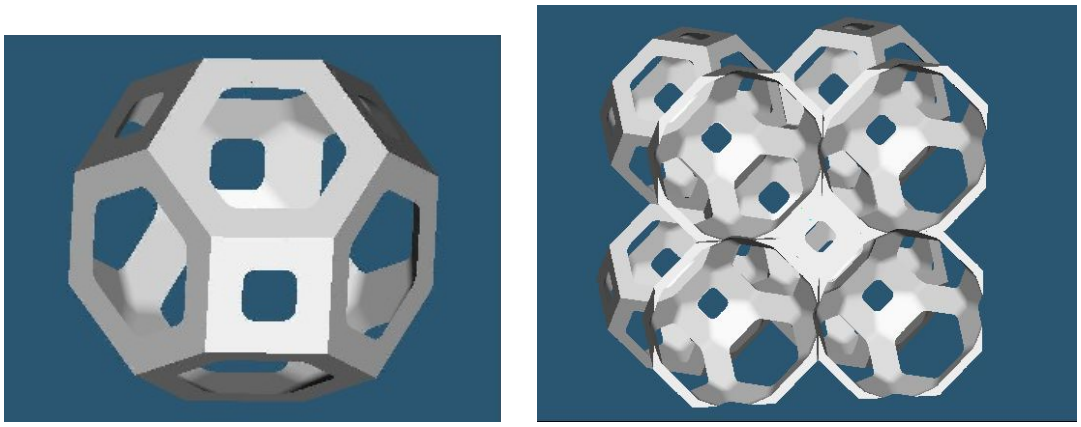

**Figure 6** Kelvin's tetrakaidecahedron. This space-filling polyhedron captures some significant features of uncompressed open-pore polyurethane.

Nevertheless, progress is underway in pore-scale fluid flow simulation. Maier et al (1999) have accomplished large-scale numerical calculation of dispersion in random-packed spherical particle beds using LBM (Lattice Boltzmann Model) techniques. Stockman (1998) also has applied LBM for small-scale dispersion prediction. Accurate large-scale simulations of fluid dispersion within open-pore cellular materials are becoming important in applications such as filtration combustion to present designers with a scaleable model of binary mixing and fluid-solid coupling effects (see, for example, Knabner (1998)).

The goals of the present research, slightly less ambitious than the preceding, include drawing the correlation between mechanical strength and fluid permeability of a few unique cellular materials in their compressed versus uncompressed and coated versus uncoated configurations. To further the existing database of compressed and uncompressed foams, we seek confirmation of the veracity of models produced from data of uncompressed ceramic-coated foam and evaluation of anisotropic properties in both mechanical compression and permeability. Macroscopic properties, as altered by compression and deposition of refractory coatings, are measured to facilitate comparison between coated foams and their uncoated substrates. Experimental data are discussed and analyzed for comparison to commonly accepted modeling relations.

## *MACROSCOPIC MECHANICS*

The materials under study, as defined by the IUPAC (International Union of Pure and Applied Chemistry), are classified as macroscopic-scale porous media, or materials with pore sizes greater than 50 nm. We use the designation of lineal pores-per-inch, or ppi, as an indication of relative uncompressed surface pore density of the substrate, with the realization that, physically, ppi is a variable that is assigned by the precursor manufacturer based upon density and flow resistance. The ppi value is therefore not necessarily representative of actual features, and is further altered by compression or densification. The achievable relative density is limited in practice by deposition rates and the time and cost to accumulate the coatings, especially as pore sizes are reduced by ligament

intrusion into the previously empty pore volume; in the present study we evaluate materials of 60% to 95% volumetric porosity.

Macroscopic, room temperature strength properties may be explicitly estimated based upon measured relative density of the porous material and its reference solid. Useful empirical simplifications have been presented by Gibson and Ashby (1997) which describe three distinct regions of mechanical response: linear elasticity due to bending ligaments, cell rupture by breaking ligaments, and ultimately, densification to a roughly non-porous state of being. Within the limited region of linear elastic bending, the beam-deformation model where $E^*/E_S \approx \left(\rho^*/\rho_S\right)^2$, and $G^*/E_S \approx \frac{3}{8}\left(\rho^*/\rho_S\right)^2$, provides explicit prediction of linear elastic tensile and compressive modulus $E^*$ and shear modulus $G^*$ as functions of relative density (the asterisk is applied by convention to designate a variable as referring to a porous vice a fully-dense solid, which is denoted by the subscript $S$).

For brittle porous ceramics, the linear elastic strain limit is small, yet if sideways deflection is restrained, in compression cellular materials can give the appearance of plasticity. This is due to the metered progress of pore collapse: the total degrees of freedom available for ligament bending aren't significantly reduced until densification begins. Results presented later illustrate the apparent plasticity available to ceramic-coated foams, especially those of high compression. The compressive crush stress of brittle foams, as derived from the linear elasticity model by extension to beam rupture, is given as $\sigma^*_{cr}/\sigma_{fs} \approx 0.2\left(\rho^*/\rho_S\right)^{3/2}$, where $\sigma^*_{cr}$ is the point of linear elastic failure and $\sigma_{fs}$ represents the fracture strength of the fully consolidated solid. Anisotropy leads to the brittle crushing ratiometric stress relation of $\frac{\sigma^*_{cr,\parallel}}{\sigma^*_{cr,\perp}} = \frac{2R}{1+\left(\frac{1}{R}\right)}$, with in-plane component $\sigma^*_{cr,\parallel}$ and thru-thickness component $\sigma^*_{cr,\perp}$. The crush strength

represents a constant value by these equations. The fracture toughness $K_{IC}^{*}$ is estimated, based upon flow size $d$, as $K_{IC}^{*} = 0.65\sigma_{fs}\sqrt{\pi l}\left(\rho^{*}/\rho_{S}\right)^{3/2}$.

While a significant catalogue of the various properties of uncompressed cellular refractory foams of approximately 100 ppi is now available, little effort has been heretofore directed into the study of compressed foams. The crush strength of uncompressed, 100 ppi SiC-coated foam as published by the manufacturer, Ultramet Inc, of Pacoima, CA, is presented in Figure 7, along with the above relation for crushing stress $\sigma_{cr}^{*}$. From Stankiewicz (2001), the manufacturer's relationship represents a statistically reliable distribution based upon data with moderate scatter. The differences in strength are attributed to the toughness of the fine-grained ceramic deposited by CVI as compared to the larger 200 μm flaw sizes used to develop the model equation of Gibson and Ashby (1997).

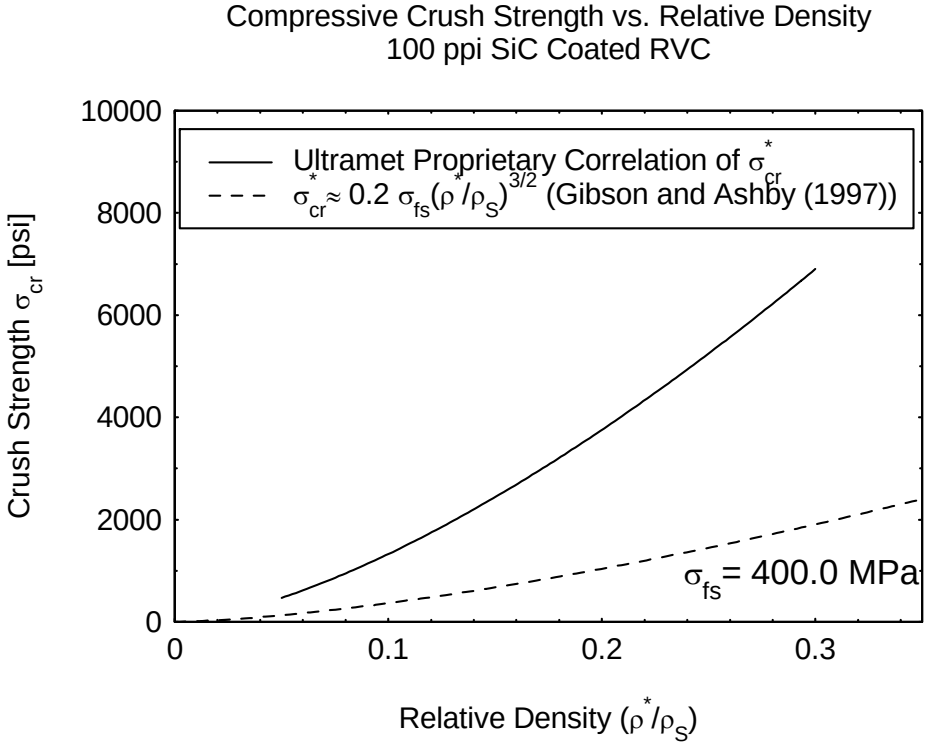


**Figure 7** Crushing resistance of uncompressed, SiC-coated cellular foam.

Stankiewicz (2001) quotes crystallite measurements of 600 to 700 angstrom (.065 μm) from unpublished research. If the flaw size $d$ is chosen based upon these values for the development of $K_{IC}^{*}$, the relation of crush strength corresponds closely to the Ultramet relation for uncompressed 100 ppi SiC-coated foam.

Heng and Sherman (1995) performed experiments on three-dimensionally compressed RVC and SiC-coated RVC as the core insulator material for a sandwiched thermal protection system; unfortunately only a single data point for compressed SiC foam exists. Their data covered the range of 65 to 100 ppi RVC foams with 3D compressions up to 400 ppi, along with a single tensile measurement of 3D compressed, 93% porous 65 ppi SiC and is presented later for comparison to measurements of uniaxially compressed RVC foam.

## *OPEN-PORE POROUS FOAM CONSTRUCTION*

The creation of an engineered refractory cellular material begins with selection of a flexible open-pore organic precursor such as polyurethane. The precursor is batch-characterized by the properties of open or closed pores, ppi, flow capacity, etc, as required. The uniformity of the precursor construction appears exceptionally good with regard to ligament sizes; as shown in Figure 8, the ligament breadths fall within a 10 μm range for the 100 ppi precursor used in the current investigation.

The flexible foam may be sequentially shaped or compressed to achieve its near-net final part shape with the desired ppi value. As received from its manufacturer, the precursor may have an inherent direction of pore stretch in the "rise" direction due to the buoyancy of the gas which was infiltrated to form the pores in the precursor's liquid state. The stretch of the pores from this artifact is typically around R~1.2. Uniaxially compressed foams are normally compressed perpendicular to the rise direction. Rigidization of the foam in its near-net manufactured shape is accomplished by resin infiltration and pyrolysis to RVC.

Coatings, if desired, are accumulated by CVI or CVD onto the common cellular RVC core substrate to create much stronger refractory foam. Coatings

show hermetic integrity and fine grain sizing as described earlier, indicating good fracture toughness. Techniques to accelerate coating deposition within moderately porous materials are viable but await further development. Melt infiltration of directly convertible resins appears promising but some development is required to protect the underlying substrate.

The RVC ligament substrate may be left intact or removed by bakeout, as in firebrick construction, for weight reduction or to isolate a fluid contained within the hollowed-out ligaments from one in the cellular interstices.

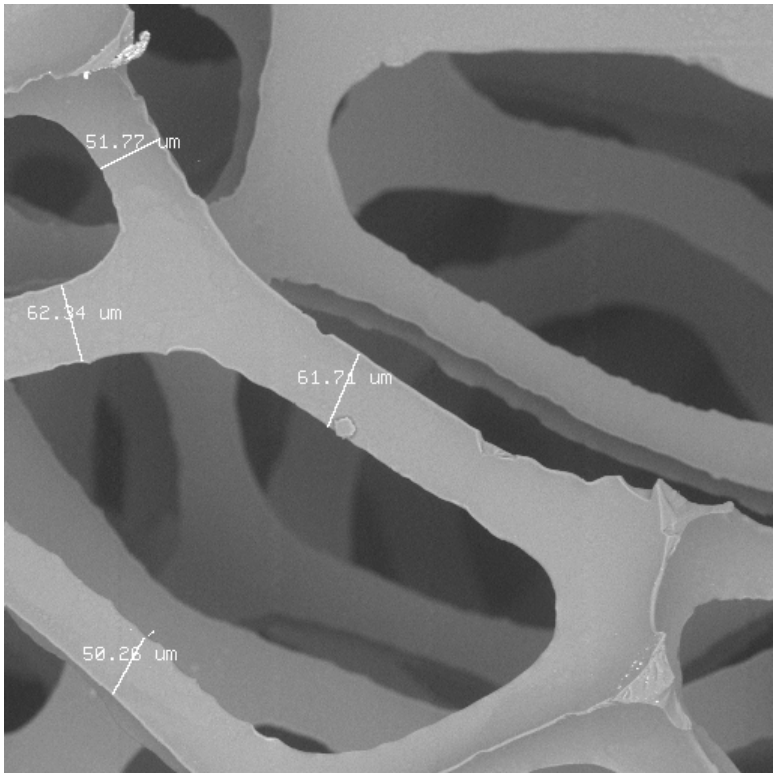


**Figure 8** Uncompressed, uncoated 100 ppi RVC, displaying average ligament breadths of 50 μm.

## *FLUID PERMEABILITY*

The combined effects of pressure, viscosity, inertia, capillary wetting, phase transition, buoyancy, density, turbulence and kinetics may all have a say in the final outcome of a fluid process within even very large-pored porous media. While fluids follow a naturally tortuous path when permeating porous media, at the typical pore-scale Reynolds number ($1 < Re < 100$), fluid advection is

normally secondary in importance to diffusion and dispersion. Some efforts have been made in extracting the empirical constants associated with high Reynolds number flow models. The experiments of Sommer (1999), using the models of Ergun (1952) and Gortyshov (1986), determined the coefficients $A$ and $B$ of the general relation $\frac{dP}{dx} = Au + Bu^m$ for coated cellular materials of 65 to 160 ppi. Despite having materials available of 2X uniaxial compression, Sommer's experiments did not observe anisotropic flow properties.

For most applications utilizing homogeneous fluids, the most important property is permeability $k$. The permeability is often modeled as a very large set of small capillary tubes. Viscous loss is, however, inextricably linked to microscopic cell structure and fluid tortuosity, as has been shown by Fand et al (1987) and others. The permeability seems best determined by direct measurement, as most experimental methods mentioned previously still require an empirical correction which may not have been validated for a particular material. The permeability tensor, contained in the conservative equations of mass, momentum and energy in porous media, including the inertial equations developed by Forchheimer (1901), Bachmat (1965), and Ergun (1952), can subsequently be applied in analysis.

## RESULTS

The materials investigated consisted of RVC and SiC-coated RVC foams as listed in Table I. Due to the method of estimating porosity based upon added coating weight, the composite nature of coated RVC foam should be stated. The predicted porosity, when compensated for the RVC core, becomes $\varepsilon = \left(1 - .03\eta - \left(\frac{\rho_U^*}{\rho_S}\right)\right)$, where $\eta$ is the compression ratio (assuming a 97% porous precursor), and $\left(\frac{\rho_U^*}{\rho_S}\right)$ the Ultramet-added fractional measure of added density. The relative density $\left(\frac{\rho^*}{\rho_S}\right)$, the primary material parameter required in the

analysis models, is slightly murky in its relation to the composite coated materials. Normally, the contribution of 97% porous, uncompressed RVC to the coated material strength is considered negligible, and the small fraction of weight from the RVC is disregarded. As is shown shortly, for the highly compressed and coated materials, the RVC core may still contribute the majority of strength. The value $\left(\frac{\rho^*}{\rho_S}\right)$ of Table I therefore represents the fractional contribution of the RVC, $\left(\frac{\rho^*}{\rho_S}\right)_{RVC}$ plus the value of $\left(\frac{\rho_U^*}{\rho_S}\right)$.

| SAMPLE (TYPE-PPI-COATING) | Compression Ratio $\eta$ | $\left(\frac{\rho^*}{\rho_S}\right)$ | $\left(\frac{\rho^*}{\rho_S}\right)_{RVC}$ | $\left(\frac{\rho_U^*}{\rho_S}\right)$ | Porosity $\varepsilon$ | |
|---|---|---|---|---|---|---|
| | | | | | Predicted | Measured |
| RVC-100 | 1 | .03 | .03 | NA | .97 | .9467 |
| RVC-200 | 2 | .06 | .06 | NA | .94 | .8949 |
| RVC-400 | 4 | .12 | .12 | NA | .88 | .8593 |
| RVC-600 | 6 | .18 | .18 | NA | .82 | .8246 |
| RVC-1100 | 11 | .33 | .33 | NA | .67 | .6668 |
| SiC-100-20 | 1 | .23 | .03 | .20 | .77 | .6701 |
| SiC-600-15 | 6 | .33 | .18 | .15 | .67 | .6136 |
| SiC-600-12 | 6 | .30 | .18 | .12 | .70 | .7010 |
| SiC-1000-5 | 10 | .35 | .30 | .05 | .65 | .6505 |

**Table I** Characteristics of materials under investigation.

The predicted porosities are presented in Table I for comparison to the porosities measured by alcohol immersion pycnometry at FMI/EMTL of Biddeford, ME. The errors in predicted porosity are attributed to non-uniform pores of the uncompressed precursor (which could be intensified during compression) or, most likely, scatter in precursor batch porosity as reported by the precursor manufacturer. The relative uncertainty of the pycnometry measurements is +/- 1.5%.

SiC-coated porous materials of 100 ppi with 20% coating, 600 ppi with coatings of 5% and 12%, and 1000 ppi with 5% coating were examined. The 100 ppi SiC-coated substrate was coated in its uncompressed state, while the 600 ppi and 1000 ppi materials were compressed by factors of 6 and 10 before rigidizing and coating. Uncoated RVC materials of 100, 200, 400, 600 and 1100 ppi were also examined. Their reported uniaxial compression ratios were, respectively, unity, two, four, six and eleven.

All samples were tested in both in-plane and thru-thickness mechanical compression. The 600 ppi and 1000 ppi SiC-coated samples were tested in lots of three in in-plane compression; all others were single lot tests to identify trends. Elastic moduli are assumed equal in tension and compression. The overlapping set of 100 and 600 ppi SiC and RVC foams was especially useful in observing the effects of the coatings upon properties.

## *Mechanical Properties of SiC-Coated and Uncoated Cellular RVC*

Unconstrained compression tests were performed at FMI/EMTL of Biddeford, Maine, using an Instron #2120 and self-aligning platens. In-plane RVC and SiC-coated RVC compression test pieces were nominally 0.50 in. x 1.00 in. full-slab thickness and 0.50 in. x 0.75 in. full-slab thickness, respectively (slab thickness was 0.50 in. (RVC) or 0.35 in. (SiC)). Thru-thickness compression test pieces were 0.75 in. square by slab thickness.

Measurements of in-plane and thru-thickness compressive strengths and estimated elastic modulus are presented in Table II. The table lists the values by component under the assumption of orthotropy. Figures 9 and 10 display the measured values of in-plane and thru-thickness crush strength as defined by the apparent limit of linear elasticity.

| SAMPLE | $\sigma^*_{cr,\parallel}$ (I.P.) | $\sigma^*_{cr,\perp}$ (T.T.) | $E_\parallel$ (I.P.) | $E_\perp$ (T.T.) |
|---|---|---|---|---|
| | [ksi] | [ksi] | [ksi] | [ksi] |
| RVC-100 | 0.03 | 0.02 | 3.6 | .50 |
| RVC-200 | 0.12 | 0.08 | 10 | 5.5 |
| RVC-400 | 0.23 | 0.09 | 25 | 6.0 |
| RVC-600 | 0.39 | 0.39 | 41 | 10 |
| RVC-1100 | 3.9 | 2.5 | 210 | 75 |
| SiC-100-20 | 3.2 | 5.3 | 560 | 280 |
| SiC-600-15 | 3.2 | 2.8 | 720 | 220 |
| SiC-600-12 | 1.7 | 2.2 | 510 | 190 |
| SiC-1000-5 | 2.2 | 2.7 | 600 | 160 |

**Table II** Measured crush strengths and elastic moduli.

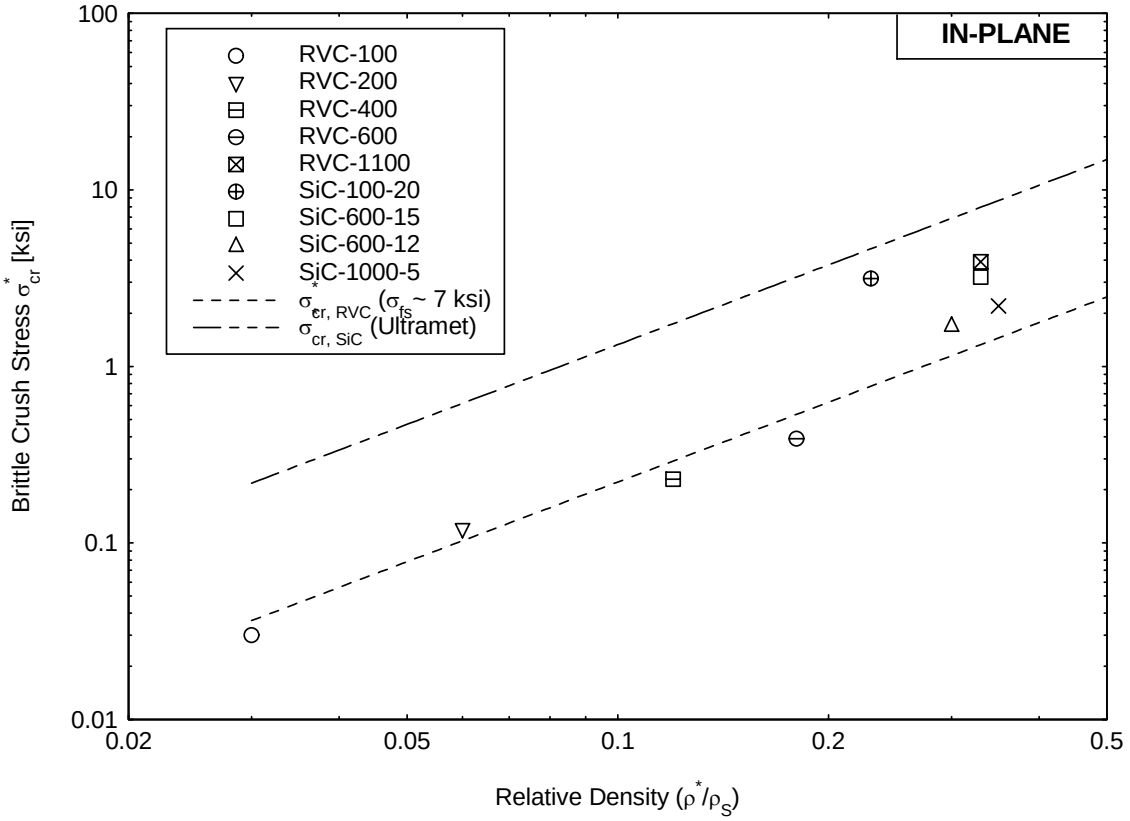


**Figure 9** In-plane crush strength results.

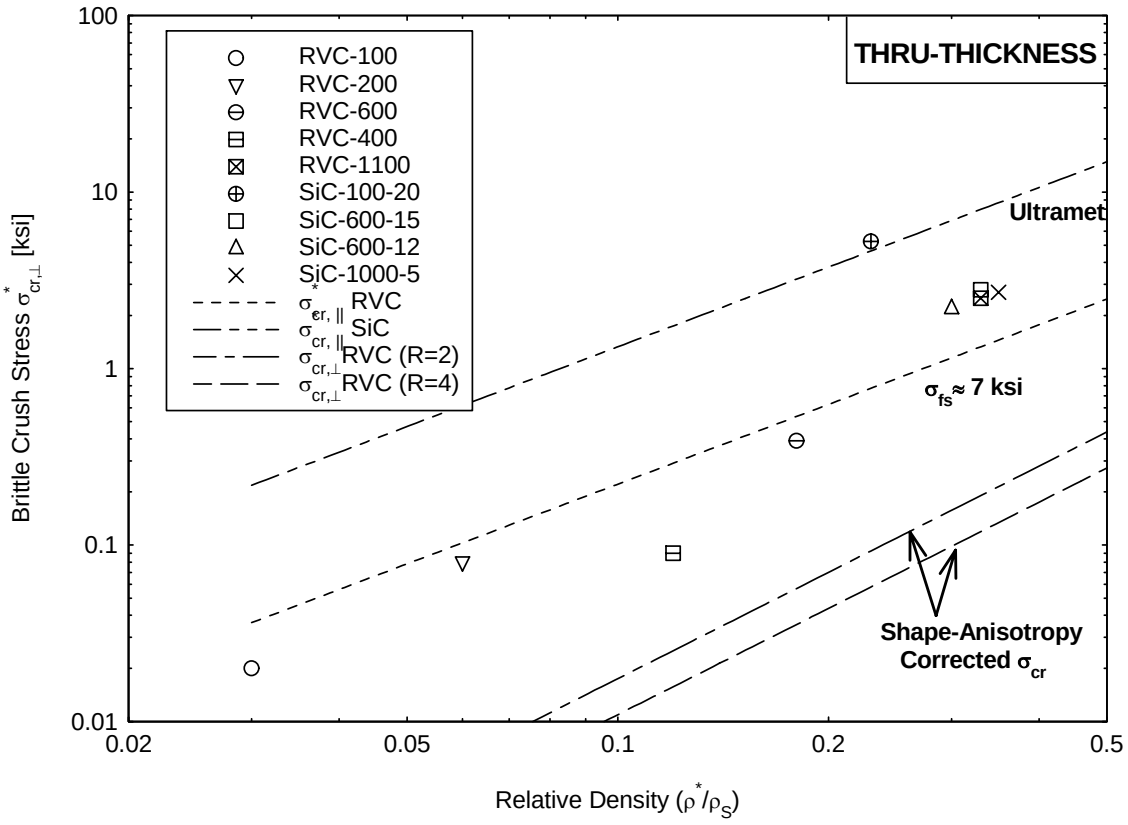


**Figure 10** Thru-thickness crush strength results.

Some observed stress responses to loading are presented in Figures 11 and 12. The distinct regions of linear elasticity seen in the graphs were used to estimate the thru-thickness and in-plane values of compressive crush strength and elastic modulus, $E_{\perp}$ and $E_{\parallel}$. Surprisingly, the elastic limits of the SiC-coated materials tested in multi-sample lots were mostly indistinguishable in sample-to-sample variation. The brittle crushing response of the coated materials, ostensibly constant from the elastic limit to densification, varied widely with deformation as shown in Figure 12.

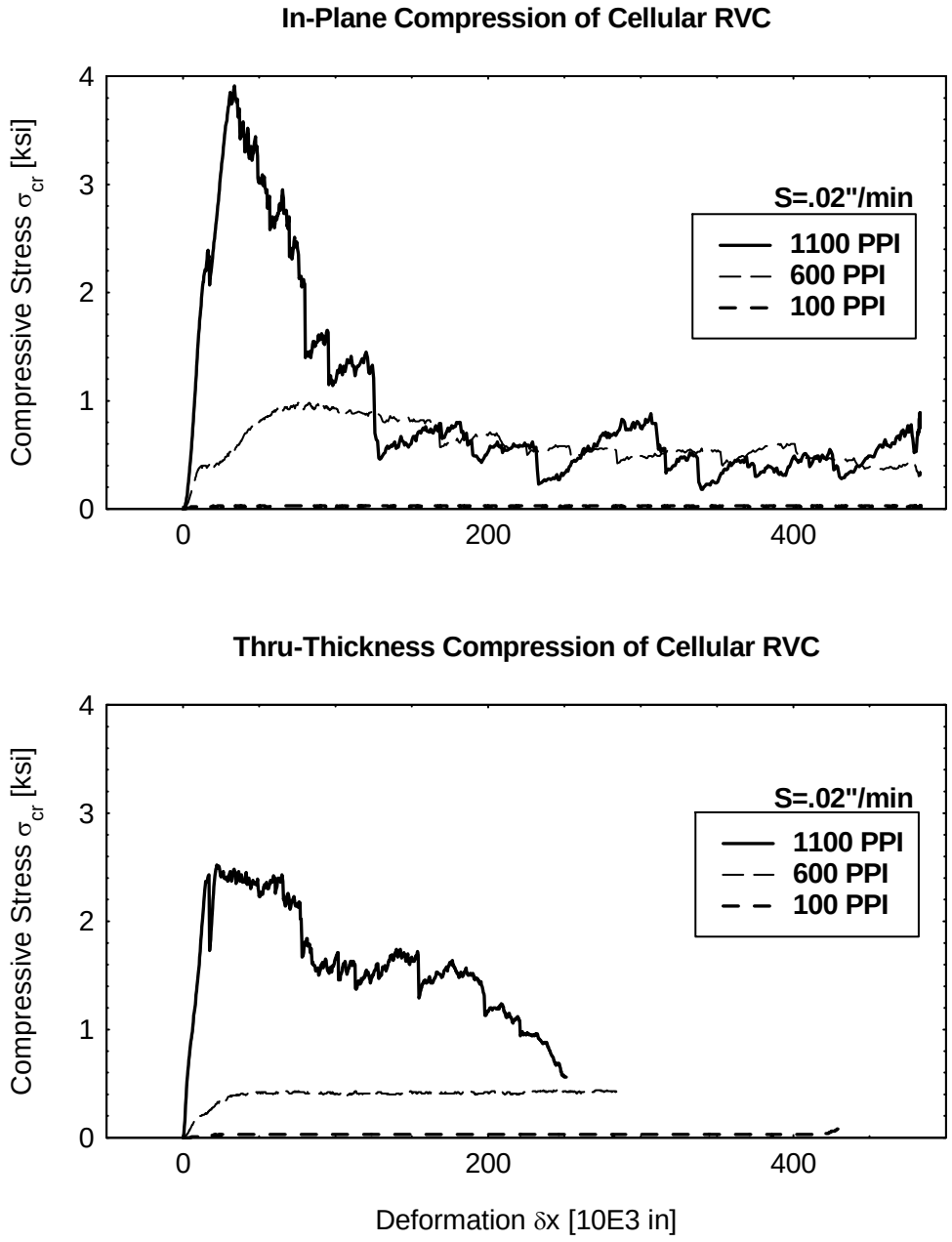


**Figure 11** Loading response of RVC materials.

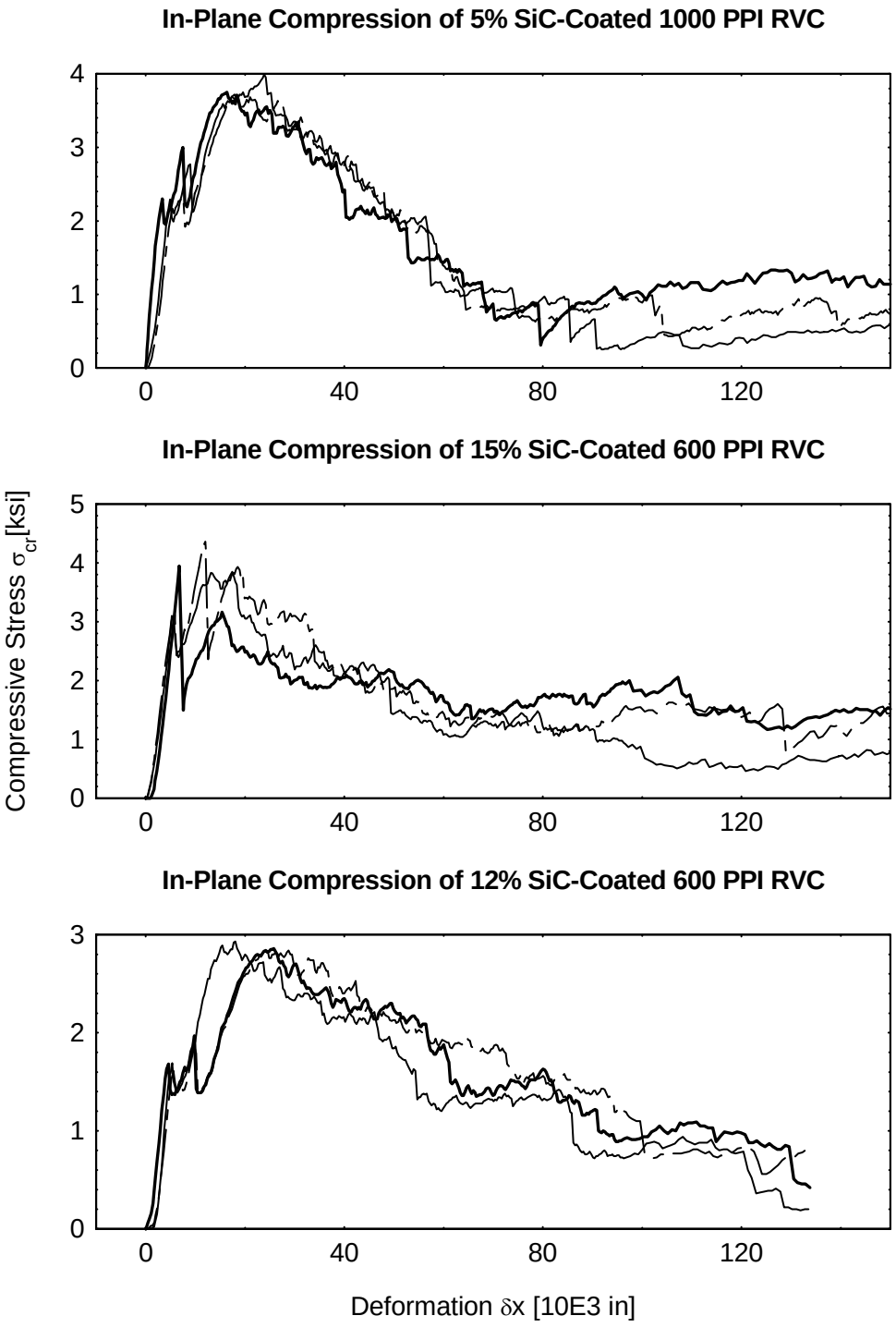


**Figure 12** Loading response of SiC-coated materials.

## *Permeability*

Permeability was calculated from differential pressure and mass flow rate measurements obtained using a simple, constant-pressure gas permeameter. Both in-plane and thru-thickness measurements were accomplished for each of the compressed materials using low flow rates to reduce entrance effects and to ensure valid Darcian flow. The samples were carefully sealed against the containment walls to preclude false readings. The uncompressed samples were assumed to be isotropic for this research.

Using Darcy's Law, $u = \frac{k}{\mu}\frac{dp}{dx}$, the permeability $k$ was estimated from measurements of mass flow rate and pressure differential. Pore Reynolds number was derived from bulk velocities with the assumption that pore velocity $u_p = \varepsilon u$, which is valid if areal and volumetric porosities are equal. Note that this assumption is invalid if blockage or inhomogeneous pore distribution is evident. The selection of pore diameter is complicated by the material's compression. A known specific surface area $S$ of 100 ppi RVC was scaled against the compression ratio and any added surface area from coating, allowing the hydraulic pore diameter to be estimated as $d_h = 4\frac{Area}{Perimeter} \approx 4\frac{\varepsilon}{S}$. $S$ of 100 ppi RVC was chosen from the calculations of Sommer (1997), and extrapolated by the compression ratio $\eta$ to the current materials. The estimated uncertainty in permeability is +/- 6%, mostly due to rotameter resolution.

Permeability values for uncoated and coated materials are presented versus Reynolds number in Figures 13 and 14. Hydraulic diameter and specific surface areas of compressed RVC foams are presented in Figure 15.

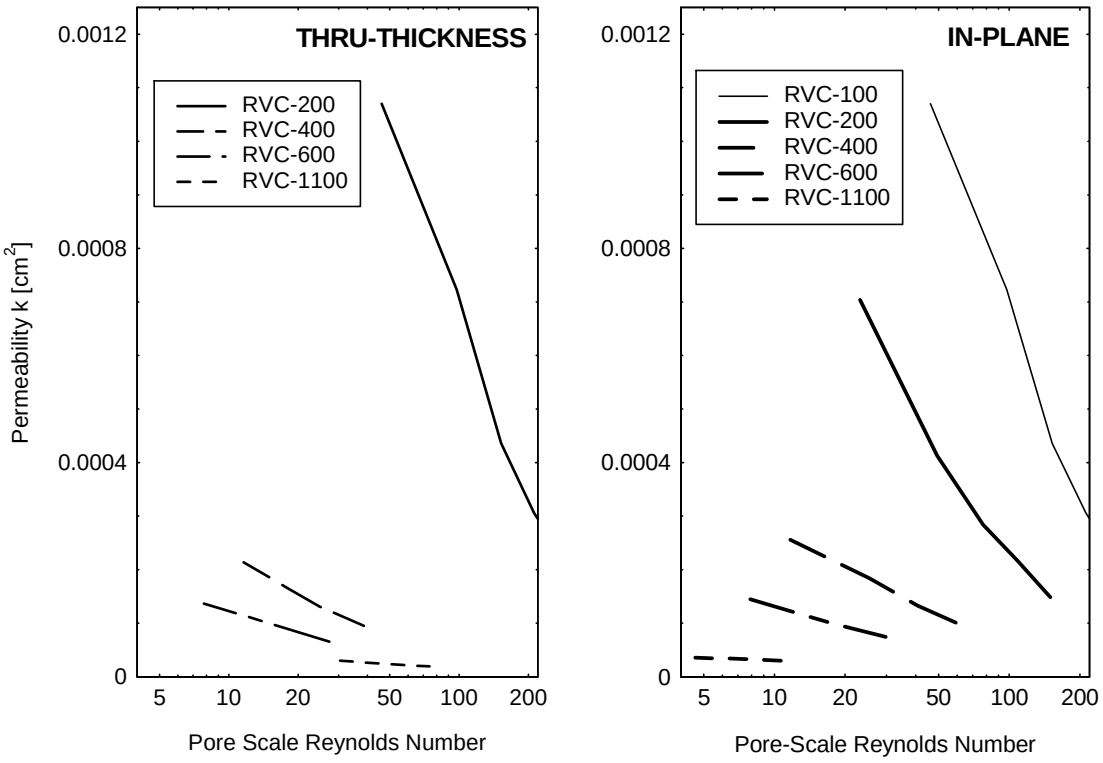


**Figure 13** Anisotropic permeability of RVC foams.

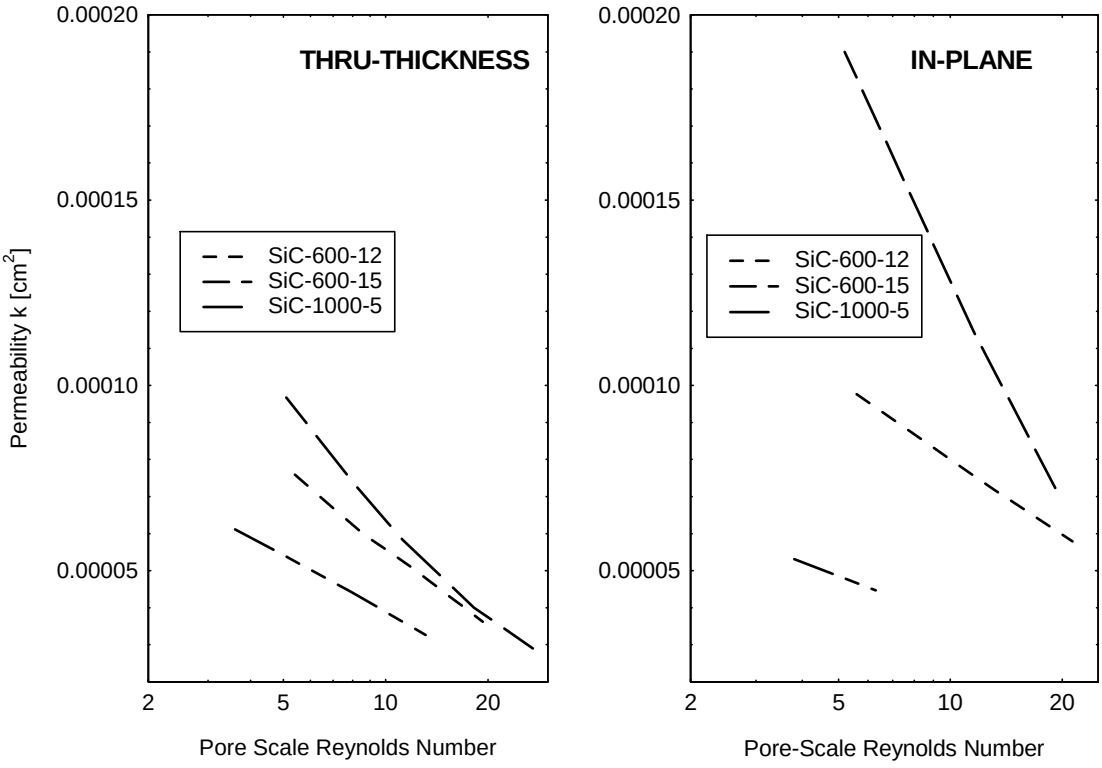


**Figure 14** Anisotropic permeability of SiC-coated RVC foams.

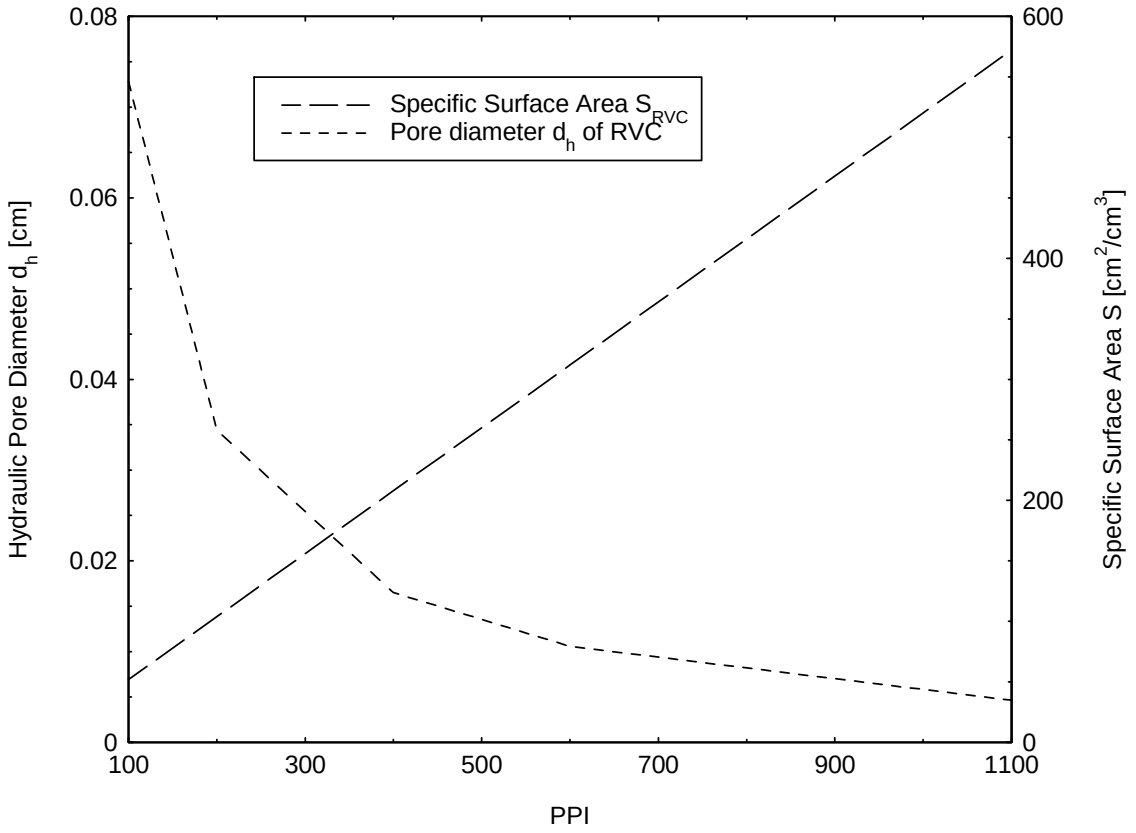


**Figure 15** Estimated hydraulic diameters and specific surface areas of compressed RVC foams.

# CONCLUSIONS

## *Mechanical Response To Coating and Compression*

The modeling relations that utilize relative density as the primary descriptive variable of mechanical properties serve well for uncoated RVC foams but lose some accuracy for highly compressed, lightly coated material. Those materials tend to have their properties bounded between the strength curves of the substrate and the pure coating.

Post-rupture mechanical loading does not follow the idea of constant crush strength consistently. This region of brittle fracture appears only for a few samples, and is further inconsistent between in-plane and thru-thickness measurements. Instead, plastic relaxation appears to dominate the majority of the materials. A possibility is that, after enough ligament rupture occurs to

present a principle directional of failure propagation, a near-constant crush strength path is followed. The anisotropy-corrected crush strength is also presented in Figure 11 for comparison to measurements. The corrected strength, as based upon the measure of shape-anisotropy from the compression ratio calculated from $\frac{\sigma^*_{cr,\|}}{\sigma^*_{cr,\perp}}$, apparently underpredicts the actual in-plane to thru-thickness strength ratios by factors up to 5.

## *Permeability and Macroscopic Material Properties*

The directional nature of gas permeability was captured in the preceding experiments. The sensitivity of permeability to compression was shown to become much less as pore density increases from compression. Thus, less-porous, generally stronger cellular materials should have a more isotropic permeability tensor, if the assumption that flow pathways are not blocked is valid. Applications using compressed cellular materials should be planned with this in mind.

ACKNOWLEDGEMENTS

The authors express much gratitude for the efforts of Dr. Ed Hare at SEM Labs Inc. of Snohomish, WA, for cheerful response to last minute imaging requests, Darrell Dunn at FMI/EMTL of Biddeford, ME, for timely and comprehensive measurements, and Ed Stankiewicz at Ultramet Inc., of Pacoima, CA for insightful discussions on cellular ceramics.

## *REFERENCES*

[1] Ashby, M. F., (1992) *Materials Selection in Mechanical Design*. Pergammon Press, Oxford UK.
[2] Bachmat, Y., (1965) Basic Transport Coefficients As Aquifier Characteristics, I.A.S.H. Symp. *Hydrology of Fractured Rocks, Dubrovnik* **1**, pp. 63-75.
[3] Bear, J., (1972) *Dynamics of Fluids in Porous Media*. American Elsevier Publishing, New York, NY.
[4] Brace, W. F. (1977) *J. Geophys. Res.*, **82**, p. 3343.
[5] Ergun, S., (1952) Fluid Flow Through Packed Columns, *Chem. Eng. Prog.* **48**, pp. 89-94.
[6] Fand, R. M., Kim, B. Y. K., Lam, A. C. C., Phan, R. T., (1987) Resistance to the Flow of Fluids Through Simple and Complex Porous Media Whose Matrices are Composed of Randomly Packed Spheres *Transactions of the ASME*, **109**.
[7] Forchheimer, P., (1901) Wasserbewegung durch Boden, *Z. Ver. Deutsch. Ing.* **45**, pp. 1782-1788.

[8] Gibson, L., and Ashby, M. F., (1997) *Cellular Solids – Structures and Properties* University Press, Cambridge UK.
[9] Gortyshov, Yu. F., Murav'ec, G. B., and Nadryov, I. N., (1987) Experimental Study of Flow and Heat Exchange in Highly Porous Structures *Inzhenerno-Fizicheskii Zhurnal*, **53**, No. 3, pp. 357-361.
[10] Heng, S. and Sherman A., (1995) *Thermal Protection For Maneuvering Reentry Vehicle (MaRV)*, Final Report, SBIR Contract F04704-92-C-0031.
*[11]* Knabner, P., and Schneid, E., (1998) Numerical Bifurcation Analysis of Premixed Combustion in Inert Porous Media, in *High Performance Scientific and Engineering Computing*, Springer Verlag, Berlin, pp. 39-50.
[12] Kozeny, J., (1927) Uber kapillare Leitung des Wassers im Boden: Sitzungsber. Akad. Wiss. Wien, **136**, pp. 271-306.
[13] Maier, R. S., Kroll, D. M., Davis, H. T., and Bernard, R. S., (1998) Pore-Scale Flow and Dispersion *Int. Journal of Modern Physics C*, **9,** No. 8, pp 1523-1533.
[14] Sommer, M., (Dec 1997) *Determination and Characterization of Hydraulic and Thermal Properties of Ceramic/Metal Porous Media*, Doctoral Dissertation, UCLA.
[15] Stankiewicz, E., Private Communication, May 25, 2001.
[16] Stockman, H. W., (1998) Accuracy and Computational Efficiency in 3D Dispersion via Lattice Boltzmann: Models for Double-Diffusive Fingering and Dispersion in Rough Fractures, *7th Int. Conf. on the Discrete Simul. Of Fluids*, University of Oxford, UK.